Nigar, H.; Sturm, GSJ.; García-Baños, B.; Penaranda-Foix, FL.; Catalá Civera, JM.; Mallada, R.; Stankiewicz, A.... (2019). Numerical analysis of microwave heating cavity: Combining electromagnetic energy, heat transfer and fluid dynamics for a NaY zeolite fixed-bed. Applied Thermal Engineering. 155:226-238. https://doi.org/10.1016/j.applthermaleng.2019.03.117

Numerical Analysis of Microwave Heating Cavity: Temperature distribution in time and space within a NaY zeolite fixed-bed

Nigar H[a]., Sturm G.S.J.[b], Garcia-Baños B.[c], Peñaranda-Foix F.L.[c], Catalá-Civera J.M.[c], Mallada R.[a,d*], Stankiewicz, A.[b], Santamaría J.[a,d*]

[a] Nanoscience Institute of Aragon and Chemical and Environmental Engineering Department, University of Zaragoza, 50018 Zaragoza, Spain

[b] Process & Energy department, Delft University of Technology, Leegwaterstraat 39, 2628 CB Delft, The Netherlands

[c] Instituto ITACA, Universidad Politecnica de Valencia, Camino de Vera, 46022, Valencia, Spain

[d] Networking Research Centre CIBER-BBN, 28029 Madrid, Spain

*Corresponding authors: rmallada@unizar.es, jesus.santamaria@unizar.es

Keywords

Modelling and numerical simulation, Dielectric properties, Microwave heating, Power dissipation, Transient temperature profiles

Abstract

Three-dimensional mathematical model was developed for the rectangular TE_{10n} cavity system. Energy/heat, momentum equations were solved together with the Maxwell's electromagnetic field equations using COMSOL Multiphysics® simulation environment. The dielectric properties, ε' and ε'', of NaY zeolite were evaluated as a function of temperature. Considering these values, the microwave heating, i.e., temperature profile along the bed, and temperature evolution with time, of a fixed-bed made of dry porous NaY zeolite was simulated, and temperature results were compared to the experimental values for the validation of the model. Furthermore, the prediction of thermal runaway and heating behavior of other materials were studied.

1. Introduction

Microwave heating, MWH, directly converts the microwave energy into heat in contrast to conventional heating, CH, transfer mechanisms that occur through a surface. The electromagnetic waves directly interact with the charges in the molecules and solids (i.e., dipoles, ions or delocalized electrons) which result in a volumetric heating of the material. MWH is characterized by a non-contact, rapid and selective heating that leads to shorter processing times. MWH is considered as an energy efficient process; although not always as it has been reported by several authors [1, 2]. Nevertheless the importance and efficiency of MWH technology is endorsed by many different processing industries, starting from food technology, material processing and sintering, coal and mining that routinely heat by microwaves as a well-established technology [3, 4]. In the last fifteen years the advances in microwave assisted synthesis/chemistry including organic synthesis and heterogeneous catalysis are becoming more important and microwave energy is presented as a tool for green chemistry [2] and process intensification [5].

Microwave driven chemical reactors often report better performance compared to its counterparts heated by conventional methods, but most of the times the differences are related with the so-called “thermal effects”, and several studies point out the non-uniform heat generation with microwave irradiation due to the spatial variations of the electromagnetic field within the sample [6-8] or non-homogeneous distribution of the material [9]. The non-uniform heating and temperature distribution can be overcome in the case of liquids basically by stirring; however, the problem still remains in the case of continuous flow reactors, and heterogeneous solid-gas phase catalytic systems. Especially, the temperature distribution within the fixed/packed-bed configuration is important for the conversion of the reactants of interest. Durka *et al.* [6] reported significant two-dimensional temperature gradients in a fixed-bed of $CuZnO/Al_2O_3$ catalysts both in axial and radial directions. They observed 60ºC difference from bottom to top in 12 mm length, and 25-45ºC from center to the wall in 24 mm of diameter. In a recent work of Horikoshi *et al.* [10] focused on the selective heating of Pd/Activated Carbon catalyst in heterogeneous systems via microwave heating for continuous evolution of hydrogen from organic hydrides. They observed a large temperature distribution along the 50 mm length of the catalyst bed. Almost a

50% drop in temperature below the 15 mm of the catalytic bed, where the dehydrogenation reaction could not take place due to the lower temperature. They claim that a more uniform distribution of electromagnetic field should lead more uniform temperature within the catalyst bed and could result in significant improvement in process efficiency while giving a high conversion yields and considerable energy saving compared to the conventional heating.

The spatial electric and magnetic field distribution inside a microwave cavity, as well as in the material processed, are the major factors for materials processing to obtain the temperature profiles of the heated sample. The study of temperature distribution in microwave heated solids has been addressed by several authors, focused on the non-uniform temperature distribution, hot and /or cold spots inside the heated material by microwave [11-14]. The numerical models include the simultaneous solution of differential equations for the electromagnetic field distribution, heat transfer and fluid dynamics with a finite element analysis with software based on finite element analysis such as COMSOL Multiphysics® [15]. To perform the simulation, the exact geometry of the cavity and material together with its three-dimensional position within the cavity are essential. The temperature gradients simulated in the case of heating pinewood, carbon, Pyrex and combinations of thereof could be as high as 800K in the case of carbon cylinders inside a wood cube of 86 mm side, from the outer side to the inner part [14]. Unfortunately, none of the works were able to validate the simulated temperature profiles with experimental temperature distribution in a 2D map. Furthermore, in all the cases constant values for the dielectric properties with temperature have been considered, but this could be of special relevance in the case of important changes on these properties that could lead to a runaway.

In the present work, microwave heating of a dry porous zeolite fixed-bed in a quartz tube was studied both experimentally and numerically in a mono-mode rectangular resonant cavity. The focus was on the study of the electric field distribution, heat generation, heat transfer, and temperature distribution. The COMSOL Multiphysics® simulation environment was used to perform the three-dimensional modelling of a mono-mode (TE_{10}) rectangular waveguide microwave heating cavity. The temperature distribution in time and space within the sample in a fixed-bed configuration was simulated in the basis of experimentally measured dielectric properties (ε' and ε'') of the NaY zeolite as a function of temperature. The simulated temperature profiles were then validated with experimental data obtained with a fiber

optic and thermographic camera and the model was used to predict possible runaway during microwave heating of zeolites as well as the heating behavior of other materials inside the cavity.

2. Experimental System

The microwave heating cavity, see **Figure 1 a**, was supplied by Sairem Iberica and consist of a solid-state microwave generator functioning at the range of 2.43 – 2.47 GHz with a 0.1 MHz step and a maximum power of 150 W, and a TE_{10} mode microwave cavity with a WR420 waveguide. The cavity was further modified with a precision 3-Stub Tuner (GA1002 model, Gerling Applied Engineering, Inc., USA) to reduce the reflected power below than 10% of the forward power. Before starting the experiments, the cavity was tuned and the mismatch was analyzed by the evaluation of S-parameters, S_{11}, which are obtained by a Network Analyzer (Agilent E5061B 5 Hz – 3 GHz) within the frequency range of 2.43 – 2.47 GHz with 0.1 MHz steps.

A fixed-bed quartz tube ($Ø_{in\text{-}out}$=7 – 9 mm) was located inside the cavity through two circular sampling ports (top and bottom). The temperature in the fixed-bed was measured with a fiber optic (range: -80 to 250ºC, Ø:1 mm, Neoptix T1 Probe) inside a capillary quartz well, see **Figure 1 c**. The temperatures reported in this chapter for the fixed bed experiments correspond to the optical fiber readings at the bottom of the fixed-bed. The surface temperature of the quartz tube was also measured by an infrared thermographic camera, (range: 0-500ºC, InfraTec, GmbH, quartz emissivity: 0.9) located in front of the side window of the cavity. The Infrared camera captures the infrared images every 3 seconds. The images are further processed with an algorithm that has been developed with the Image Processing Toolbox® of MATLAB [16] to extract the quartz tube surface temperature, e.g., transient average, maximum or both. **Figure 1** shows in detail the experimental setup of the microwave heating cavity with the dimensions and the fixed-bed configuration.

The heated solid was a commercial zeolite Y powder, CBV100, supplied by Zeolyst, containing 13.0 wt.% of Na^+ as an extra-framework cation. The fine powder, without any post-treatment, was first pelletized with a laboratory press using a stainless-steel mold (13 mm in diameter). Then the pellets were crushed and ground to 80-150 μm in order to prevent compaction of the fixed bed (200 mg, 80-150 μm, L=10 mm, $Ø_{in}$=7 mm). Before the heating experiments, the fixed-bed was regenerated by

microwave heating while passing N_2 (100 ml/min, 99.9999% pure, Praxair), meanwhile, the water concentration was registered by an on-line quadrupole mass spectrometer (OmniStar, GSD 320, Pfeiffer Vacuum) to ensure that total dehydration of the sample was reached for a given set of conditions.

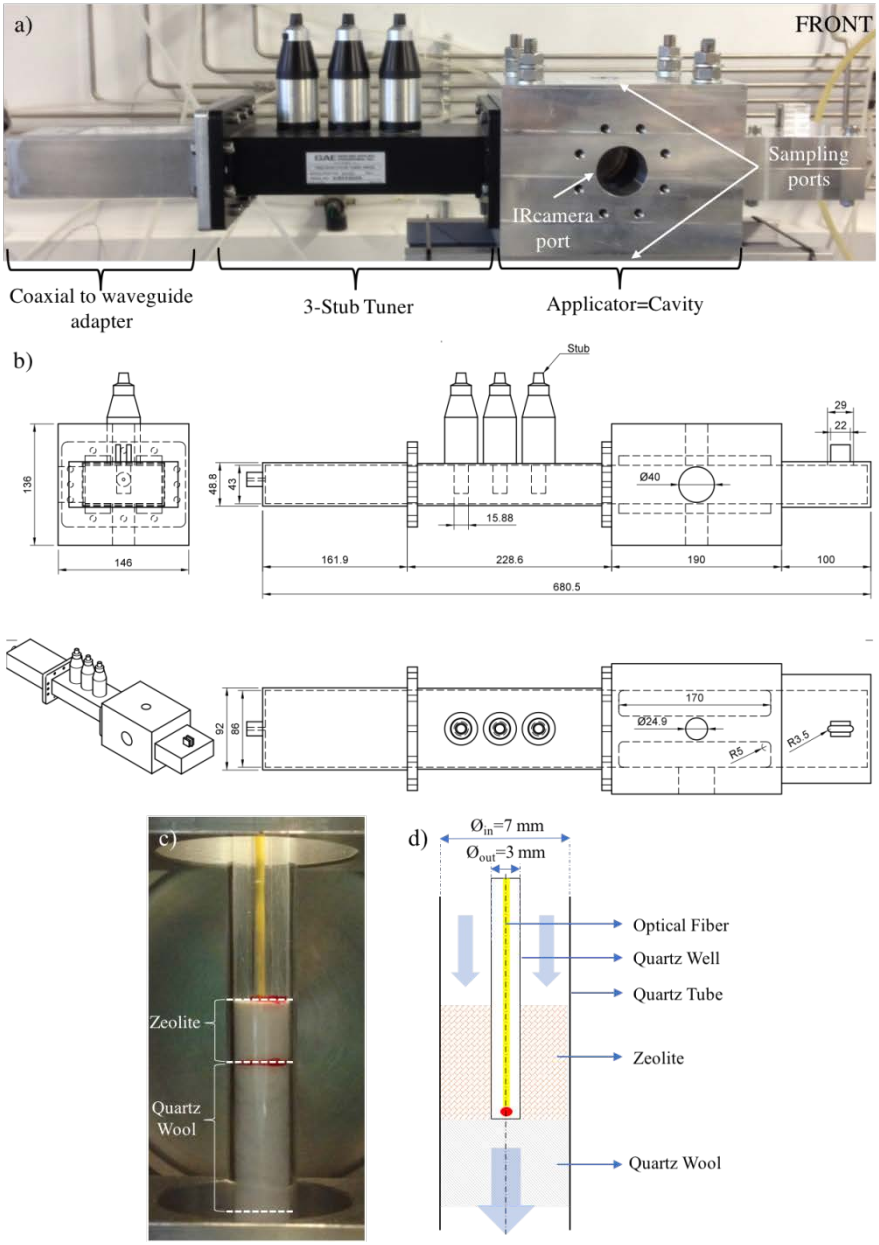

Figure 1. *Experimental setup, a) Microwave heating cavity b) The first-angle projection of 3D modelled empty Microwave Heating Cavity, the dashed lines indicate hidden edges and corners, measurement in mm c) Fixed-bed quartz tube and its corresponding d) schematic view*

2.1. Dynamic measurement of dielectric properties

The ability of a material to absorb microwave energy and transfer it into heat is governed by its dielectric properties [17]. The complex relative permittivity is defined as:

$$\varepsilon_r = (\varepsilon_r' - j\varepsilon_r'') \quad (1)$$

where ε_r' is the real part of the complex relative permittivity is known as dielectric constant, which characterizes the polarization of a material in response to an applied external electric field and it is also a measure of dielectric materials to ability to store electrical energy [18-20], whereas the imaginary part, ε_r'', is the dielectric loss factor also known as dissipation factor, which reflects the loss in the medium due to the damping vibrating dipole moment [20], which generates heat. These properties are crucial to the prediction of the spatial distribution and dissipation of electromagnetic wave fields. It is a challenging task to obtain sufficiently accurate values since they are highly dependent on temperature, moisture, frequency, the physical state either solid or liquid and composition [3, 19].

Dielectric properties (ε_r' and ε_r'') of zeolites were measured with a dual-mode microwave system recently developed by Catala-Civera et al. [17]. The equipment allows dielectric measurements of materials during microwave heating in real time. Two separate microwave sources are used for simultaneously heating and measuring, and a cross-coupling filter is used to isolate the two modes (TE_{111} and TM_{010}) from each other.

As the dielectric properties of the samples depend on temperature, the resonant frequency and quality factor of the cavity varies with temperature. From these two values, the dielectric properties of the sample are computed with an enhanced Cavity Perturbation Method [17]. To ensure an efficient power delivery and to maintain the desired heating rate a control loop ensures that, the sweep frequency bandwidth of the heating source is adjusted continuously to track the resonant peak of the cavity during the heating cycle.

The sample is inserted into the cavity through a cut-off hole at the central plane of the top wall. The test sample is placed in a quartz vial with inner diameter 10 mm and external diameter 12 mm, which can handle temperatures of up to 1300ºC. The zeolite sample has a bed size of 10 mm diameter and 15 mm height to ensure a uniform

electric field distribution in all the sample volume and thus uniform processing. The temperature of the sample under test is measured by an infrared radiation (IR) thermometer with 0.1ºC accuracy, positioned outside of the cavity and connected to it via a window in the sidewall. Since the IR thermometer measures the holder surface temperature, a calibration process was applied to find the relationship with the bulk temperature of the sample [17]. Before any measurement, the zeolite was dried overnight in an oven at 250ºC; then the measurements were done with a cycle of heating and cooling of the sample under nitrogen flow to minimize the effect of adsorbed ambient moisture. An additional second cycle of heating and cooling was performed to ensure complete drying.

3. Mathematical Model

The 3D-finite element model couples together electromagnetic waves, heat transfer and fluid dynamics. **Figure 2** shows the perspective and cross-sectional views of the model, implemented flow models, and dimensions of the quartz tube and **Table 1** represents the characteristics of the simulated system. Flanges and the outer parts of the stub tuner were not included into the model in order to reduce the complexity of the simulation, and because their effect on the overall heat balance is expected to be negligible.

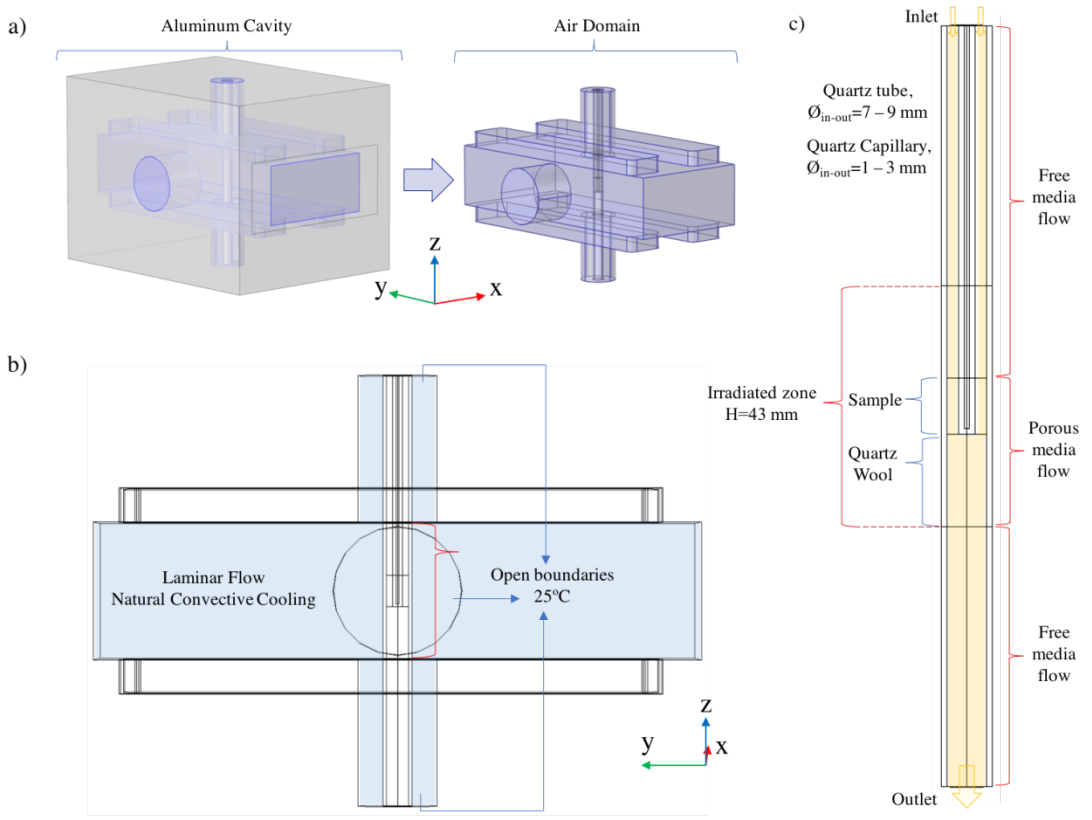

Figure 2. *a) Perspective and b) cross-sectional views of the cavity and c) quartz tube and applied flow models, i.e., laminar, free and porous media flows*

Following governing equations were used for each physic module:

3.1. Electromagnetic Waves

Maxwell's electromagnetic field distribution and the general volumetric power dissipation are calculated by solving the following equations [20-22]:

$$\nabla^2\mathbf{E} + \omega^2\varepsilon\mu\mathbf{E} = 0 \quad (2)$$

$$Q_{MW} = \pi f \varepsilon_0 \varepsilon_r'' \mathbf{E^2} \quad (3)$$

where $\mathbf{E}$ (V/m) is the electric field vector, $\omega = 2\pi f$ (s^{-1}) is the angular frequency, and ε, μ stands for the permittivity and permeability of the media.

The wave equation, Eq. (2), is solved inside the microwave heating cavity (air domain), zeolite fixed-bed and quartz tube, in this physic interface some assumptions have been made:

i. Since there is no magnetic material, the magnetic permeability of all the materials is assigned as free-space, $\mu_r = 1$, which gives no magnetic field contribution for the volumetric power dissipation.

ii. Since the electromagnetic field penetrates a negligible distance into the metallic walls, the 3D wave equation is only applied in the air domain inside of the waveguide and inside the fixed-bed and quartz tube. It was found by preliminary modeling that the energy balance was not correctly represented if a perfect electrical conductor (PEC) boundary condition was employed due to the relatively low electromagnetic dissipation inside the fixed-bed. Thus, an impedance boundary condition was assigned to the metal walls of the microwave heating cavity to account for the electric surface current present in them.

iii. Experimentally measured dielectric properties, ε' and ε'', of the sample are introduced as a function of temperature.

3.2. Heat Transfer

This module is applied inside the microwave heating cavity (air domain), as well as the fixed-bed and the quartz tube. Heat transport equation incorporates the conversion of microwave energy to thermal energy, as well as the thermal losses to the environment through the quartz tube. In this physic interface following transient equation is solved for the porous fixed-bed (solid-fluid system), quartz tube and surrounding air [23] simultaneously:

$$\rho C_p \frac{\partial T}{\partial t} + \rho C_p \mathbf{u} \cdot \nabla T + \nabla \cdot (-k \nabla T) = Q_{MW} \tag{4}$$

where ρ, C_p, k are the density, heat capacity and thermal conductivity of the fluid/solid, respectively. The symbol $\mathbf{u} = (u, v, w)$ stands for the flow velocity vector field for the x,y,z directions. First term on the left side is the rate of heat accumulation, and the second and third terms are convective and conductive contributions to heat transfer. On the right-hand side is the volumetric power dissipation, which was calculated with the electromagnetic waves module. The following assumption in this module have been made:

i. Effective average volumetric heat capacity, $C_{p_{eff}}$, at constant pressure and effective average thermal conductivity, k_{eff}, of the solid-fluid system can be used to describe heat transfer in porous media, hence Eq. (4) was modified accordingly.

ii. In the quartz tube, only conduction phenomenon was considered, $\mathbf{u} = 0$

iii. Material properties such as thermal conductivity and the heat capacity of the zeolite are considered temperature independent.

iv. A continuity condition was applied to the interface between two different domains 1 and 2: $-n \times (-k_1 \nabla T_1) - n \times (-k_2 \nabla T_2) = 0$ [24].

v. The heat flux by radiation is negligible (<0.2W).

vi. The convective velocity field around the fixed-bed quartz tube can be simulated with fluid dynamics to account for natural convection.

vii. Heat loss of the metallic walls can be neglected.

3.3. Fluid dynamics

Two physics interfaces were used in this module; *Free and Porous Media Flow* was adapted for the tubular fixed-bed due to nitrogen flow through the porous sample and *Laminar Flow* for the air domain around the quartz tube due to the natural convective cooling. The fluid dynamics are represented as time-dependent compressible fluid flow according to the following equations [25]:

$$\rho \frac{\partial}{\partial t}\mathbf{u} + \rho(\mathbf{u} \cdot \nabla)\mathbf{u} = \nabla \cdot \left[-p\mathbf{I} + \mu(\nabla \mathbf{u} + (\nabla \mathbf{u})^T) - \frac{2}{3}\mu(\nabla \cdot \mathbf{u})\mathbf{I}\right] + \mathbf{F} \quad (5)$$

$$\frac{\partial}{\partial t}\rho + \nabla \cdot (\rho \mathbf{u}) = 0 \quad (6)$$

$$\frac{\rho}{\epsilon_p}\left(\frac{\partial}{\partial t}\mathbf{u} + (\mathbf{u} \cdot \nabla)\frac{\mathbf{u}}{\epsilon_p}\right) = \nabla \cdot \left[-p\mathbf{I} + \frac{\mu}{\epsilon_p}(\nabla \mathbf{u} + (\nabla \mathbf{u})^T) - \frac{2\mu}{3\,\epsilon_p}(\nabla \cdot \mathbf{u})\mathbf{I}\right] - (\mu \kappa^{-1})\mathbf{u} \quad (7)$$

Eq. (5) stands for the free flow in the quartz tube and the laminar flow for the air domain, see **Figure 2 b-c**. The first and second terms on the left-hand side are acceleration forces, and on the right side, there are pressure gradient and viscous forces. Conservation of mass is expressed by the continuity equation, Eq. (6), which is derived by considering a unit volume of the medium and it states that the rate of increase of the mass of the fluid within an elementary unit equals to the net mass flux into the volume. Eq. (7) was used to describe the flow in the porous region, known as the *Brinkman equation* which is a combination of the continuity equation and the momentum equation. In this equation, ϵ_p and κ stand for the bed porosity and permeability, respectively, see **Table 1** [25, 26]. Following assumptions have been made:

i. The nitrogen flow rate, 100 mL/min, and the pressure, 1 atm, are fixed at the inlet of the quartz tube.

ii. No slip conditions, on the cylindrical wall of the quartz tube, $\mathbf{u} = 0$

iii. The convective velocity field around the quartz tube is computed by applying a laminar flow model, taking into account the Rayleigh number

criteria ($\mathrm{Ra=Gr\cdot Pr} < 1\times10^{9}$), where Gr and Pr are the Grashof and Prandtl numbers, respectively.

iv. A vertical buoyancy force term related to the thermal expansion is also included in eq. (2.4) for the air domain around the quartz tube: $\mathbf{F} = -\mathrm{g}\left(\rho_{air} - \rho_{air,ref}\right)$ [N/m^3], where g is the gravity (9.81 m/s^2) and ρ and ρ_{ref} are the density and reference density of air, respectively (at atmospheric pressure and 25ºC).

v. Compressible flow, ρ is variable, model is assigned for air and nitrogen domains [27].

Table 1. Characteristics of the simulated system

Fixed-bed		**Reference**
Height, H (m)	0.010	-
Inner diameter, D_i (m)	0.007	-
Outer diameter, D_o (m)	0.009	-
Bed density, ρ_{bed} (kg m^{-3})	672	-
Bed porosity, ϵ (-)	0.375 *	[33]
Bed permeability, κ (m^2)	1.15×10^{-11} **	[34]
Quartz tube		
Quartz density, ρ_w (kg m^{-3})	2200	[35]
Dielectric constant, ε′(-)	3.78	[35]
Heat capacity, $C_{p,w}$ (J kg^{-1} K^{-1})	712	[35]
Thermal conductivity, k_w (W m^{-1} K^{-1})	1.96	[36]
Particles, NaY zeolite		
Average diameter, d_{NaY} (m)	1.15×10^{-4}	-
Dielectric constant, ε′(-) and loss factor ε′′(-)	f(T) ***	-
Heat capacity, $C_{p,s}$ (J kg^{-1} K^{-1})	836	[37]
Thermal conductivity, k_s (W m^{-1} K^{-1})	0.15	[38]
Air and Nitrogen		
Dielectric constant, ε′(-) and loss factor ε′′(-)	1 and 0	-

*calculated using empirical expression of Pushnov for sphere grains

** calculated using empirical expression of Rumpf and Gupte for sphere packings

*** experimentally measured at 2.45 GHz as a function of temperature

4. Results and Discussions

4.1. Dynamic measurement of dielectric properties

The measured dielectric properties at 2.45 GHz of NaY zeolite as a function of temperature is shown in the **Figure 3.** When the zeolite is dehydrated (>250ºC), the relaxation mechanism related to microwave heating is linked to the mobility of extra-framework cations to different ion exchange positions [28-30]. In this manner, Legras *et al.* [28] studied the dielectric properties for partially and fully hydrated FAU type zeolites in the 0.5 to 20 GHz microwave region at a fixed temperature of 20ºC. At low water loading, they observed a relaxation mechanism at peak frequencies between 1.4 to 1.6 GHz, which could be extended to 2.5 GHz with 15% changes in the loss factor. This mechanism is related to the phenomenon called space charge polarization that can be produced by the separation of mobile positively and negatively charged particles under an applied electric field. In the case of zeolites, the negative charge is in the oxygen atoms of the structure and the positive corresponds to extra-framework cations. Since the NaY zeolite contains 13.0 wt.% of Na^+ as an extra-framework cation, its contribution to the dielectric properties of low silica zeolite is the major phenomenon at 2.45 GHz. According to the analyses, see **Figure 3,** the loss factor increased exponentially with temperature (>300ºC), as a consequence of the fact that, as temperature increases, the motion of Na^+ increases. This corresponds to thermal runaway and is observed during experimentation. The applied microwave power needs to be controlled properly in order to avoid the thermal runaway [28, 31, 32].

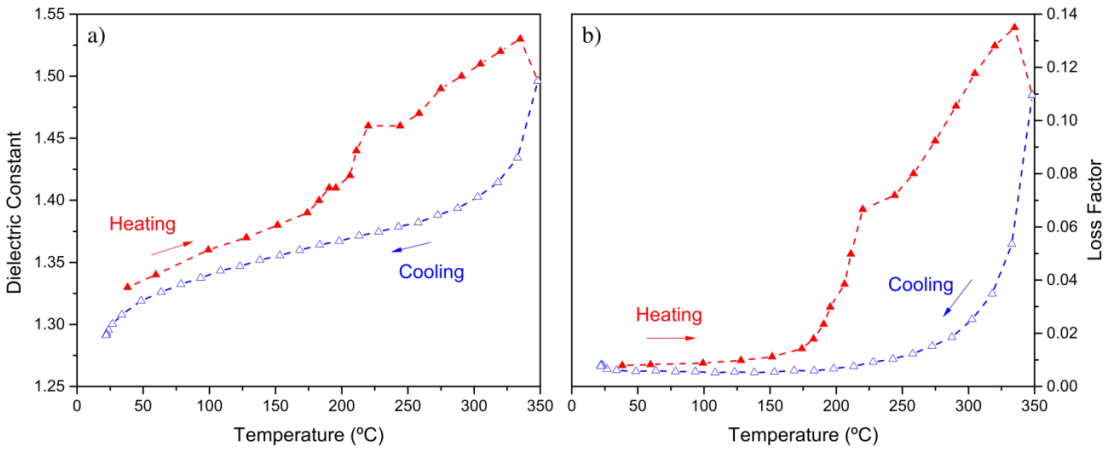

Figure 3. *Dielectric properties of NaY zeolite a) Dielectric constant b) Loss factor as a function of temperature.*

4.2. 3D-finite element model, electromagnetic field distribution

Reflection spectrums, S_{11} parameters, were experimentally measured and simulated with the regarding immersion depths of *stub 1*=25.44 mm, *stub 2*=27.57 mm and *stub 3*=8.48 mm, see **Figure 1**. The comparison between the measured and simulated data of S_{11} parameters are presented in **Figure 4**. A shift in resonance frequency in the reflection spectrum is apparent between the empty and the cavity loaded with the quartz tube; resonance occurs at the frequency of minimum reflection. As the quartz tube was introduced inside the cavity it interacts with the electromagnetic field and changes its resonant behavior, the effect of which is apparent throughout the cavity and can therefore be registered at the cavity port as a change in the S_{11} parameter. The same phenomena were also observed in the simulation with only a slight difference (magnitude and the frequency) in the case of loaded cavity. These matching spectral response and impedance matching characteristics show that the behavior of the microwave model agrees well with the physical setup which results in the validation of the model from the electromagnetic point of view.

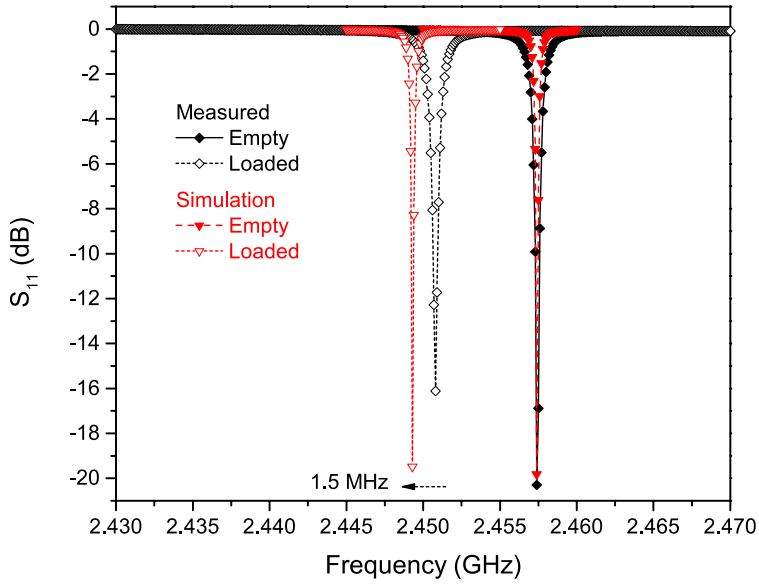

Figure 4. *Measured and Simulates S11 parameters (reflection spectrum) of empty and loaded cavity*

The cross-section views of normalized electric field distributions along the y-direction inside the empty and loaded cavity are presented in **Figure 5**. The introduction of the fixed-bed quartz tube affects the electric field distribution but the effect is not large due to the small size of the fixed-bed and the low values of the dielectric constant of the sample. This is also apparent in the relatively small shift in resonance frequency,

see **Figure 4**. The highest electric field intensity was observed at the frontier between the sample and the quartz wool (see **Figure 5 d**). This simulation also reveals that the maximum electric field intensity of the standing wave practically coincides with the fixed-bed quartz tube location because of the physical design of the cavity. This maximal region cannot be displaced to the center of the sampling windows, due to the absence of a movable shorting plate/reflector and microwave generator limitations (spectral band: 2.43-2.47 GHz).

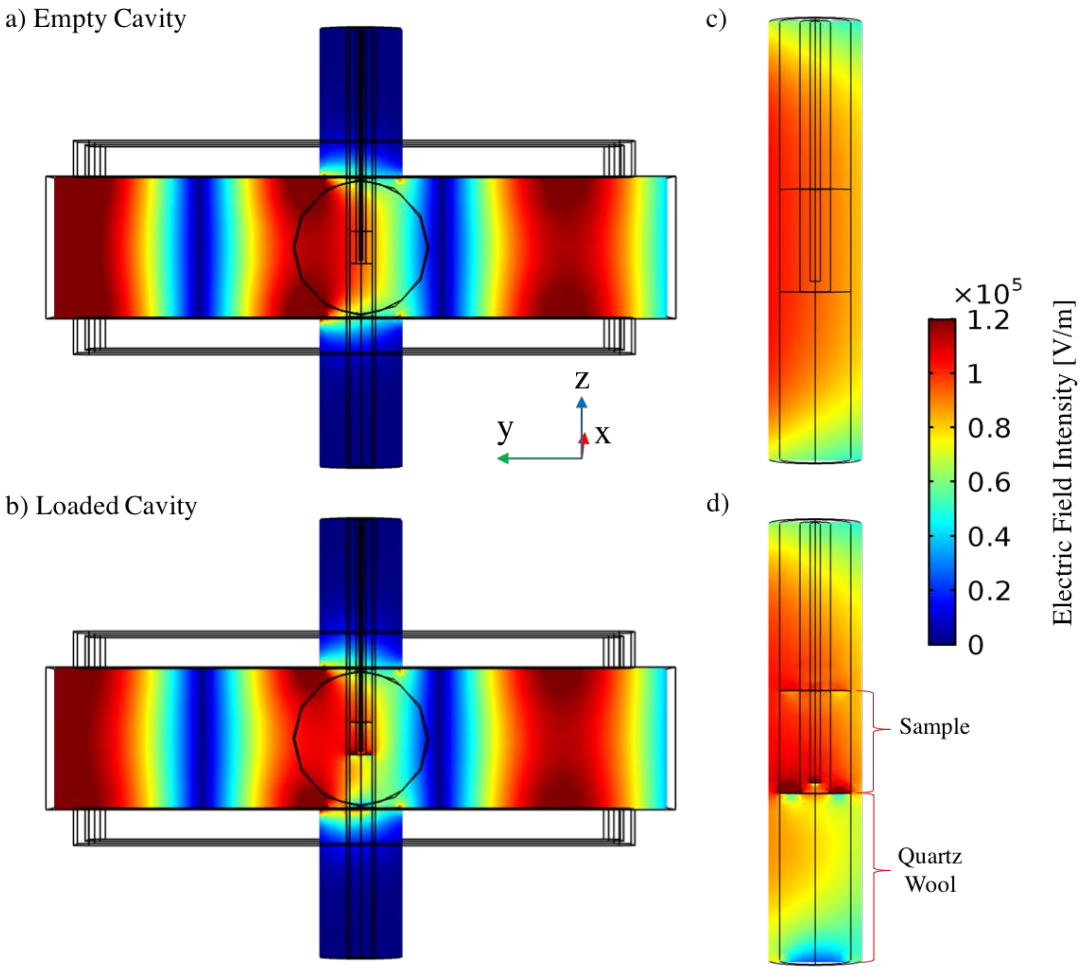

Figure 5. *Simulated electric field distribution inside the a) empty and b) loaded cavity and close look to corresponding quartz tube locations inside the cavity when it is c) empty and d) loaded. For clarity, in b) and d) quartz tube and fixed-bed domains are maintained in the case of empty cavity with the properties of air (ε′=1, ε″=0, μ_r=1, and σ=0) to have the same number of elements.*

4.3. 3-D finite element model, temperature distribution

The experimental fixed-bed temperature data was registered by the fiber optic at the bottom of the sample, where the temperature was highest, and the infrared camera was used to measure the outer surface temperature of the quartz wall. Transient

temperature profiles show that the simulated data are in good agreement with the experimental ones, as shown in **Figure 6**, where the predicted maximum temperatures for the fixed-bed and the quartz wall are represented, respectively. The average percentage relative errors between the simulation and the experimental data of the fixed-bed and the surface temperatures were ±10.3% and ±13.4% , respectively. Simulated temperatures data are higher than the experimental ones; this discrepancy could be attributed to the material properties such as thermal conductivity of the zeolite and quartz tube. In the case of zeolites, various thermal conductivities have been reported by many researchers, some of them ranges in between 0.15-0.30 W/(m.K) [33-36] which results in simulated final temperatures of 203 and 173ºC, respectively, see **Figure S1**-Supporting information.

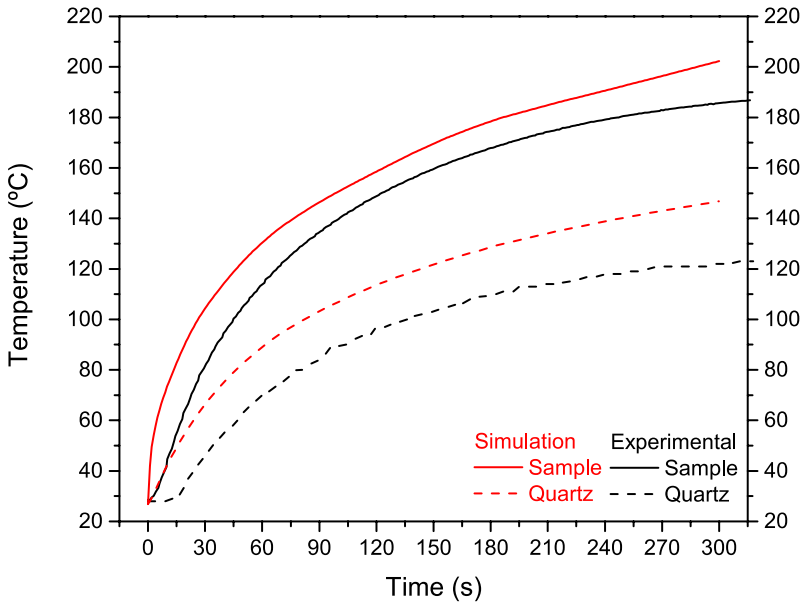

Figure 6*. Comparison of the experimental measurements and simulation predictions of transient maximum temperature profiles of the fixed-bed (measured with the fiber optic) and the quartz wall (measured with the infrared thermographic camera)*

Figure 7 shows the surface temperature of the quartz wall measured by an infrared camera at different time periods and the corresponding simulated data. The predictions are in good agreement with experimental data; in both cases, the sample starts heating from the center and then it expands axially. Even though the infrared camera has a limited resolution (320x240 pixel), it can be observed that the left side of the quartz tube has a slightly higher temperature (**Figure 7 b**, at 30s, ca. 2ºC).

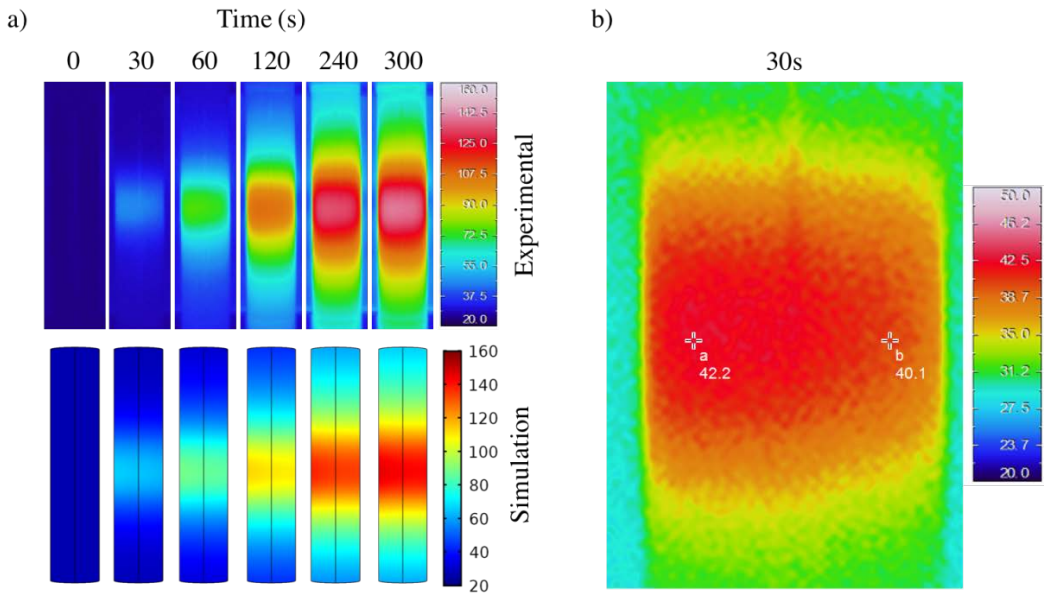

Figure 7. *Infrared images of the quartz surface temperature at different time periods and corresponding simulated data, b) an infrared image at 30s, color legends are in ºC.*

Figure 8 shows the simulated radial temperature distribution inside the quartz tube as well as along the sample at steady-state. The radial temperature profiles show that the temperature is considerably lower at the outer layers, compared to the center of the quartz tube. This is because of heat is absorbed in the volume of the sample under microwave irradiation and then lost by natural convection along the surface of the quartz tube to the surroundings. **Figure 8** also shows the variation of radial temperature profiles at different heights in the fixed-bed quartz tube. There is a slight temperature increase, ca. 2-4ºC, at the left side (1-3 mm, towards the generator side) of the sample in comparison to the right side (6-8 mm). This is in accordance with the electrical field distribution in the cavity, which is not centered within the fixed-bed, explained previously, see **Figure 8 c**. Despite a distribution that tends towards the generator side, the overall distribution is roughly symmetrical, i.e., the asymmetry of the microwave field is smoothed out by heat transfer. The temperature difference is less pronounced at the top (H=10 mm) compared to the bottom of the sample (H=0 mm), and the bottom part is hotter than the top, ca. 40 ºC. The maximum radial temperature is reached near the fiber optic location, 4-5mm. This temperature gradient is linked to the non-uniform electric field distribution inside the sample, and the heat transfer dynamics in the system. It should be noted that the high-temperature region corresponds to the relatively high electric field region, see **Figure 8 b** [18, 37]. Despite this electric field gradient, it

was observed that 58% of the fixed bed has the temperature range in between 160-197ºC.

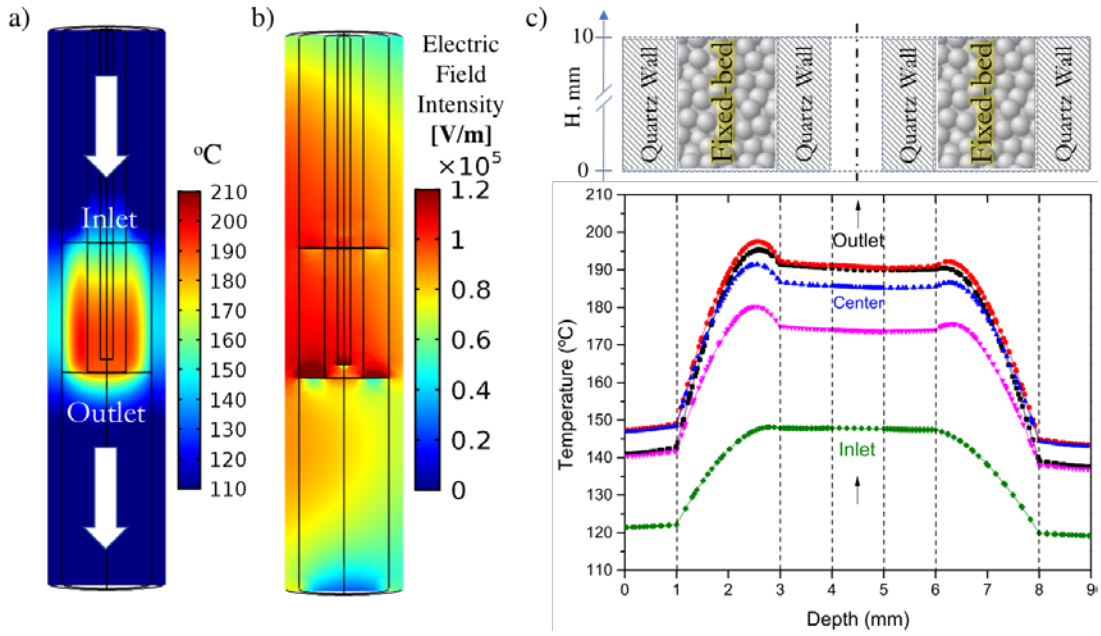

Figure 8. *Simulated cross-sectional view of the a) quartz tube fixed-bed and its corresponding b) electric field distribution c) spatial temperature distribution at steady-state.*

4.4. Energy Balance

The overall energy balance in the microwave heating cavity and the fixed-bed shows that only 6.2% of the input power was dissipated within the NaY zeolite fixed-bed, with a reflection loss of 1.2%. This means that the rest of the microwave energy was dissipated in the metallic cavity wall due to electric currents. The efficiency of this microwave heating cavity is very low, and this could be due to the small volume of the NaY zeolite fixed-bed (0.31 mL with respect to the whole cavity volume, 2.8 L) in the microwave heating cavity. A similar conclusion was reached by Coss et al. [38], only 27% of the input power was absorbed in their case, even though they used a larger bed of a good microwave absorber, granulated activated carbon and the adsorbent volume=18.8 mL. The authors expected that this efficiency could become higher with the larger volume of adsorbent. Also, Cherbanski [39] calculated the efficiency factor using 13X zeolite in a multi-mode cavity, giving a 21% efficiency (absorbent volume=253 mL). We decided to simulate larger volumes of the same adsorbent, in our microwave heating cavity, to predict its efficiency. The inner diameter of the quartz tube was increased from 7 mm (V:0.31mL) to 10 (V:0.71 mL) and 14 mm (V:1.47 mL).

Figure 9 represents the parametric analysis, power dissipation and corresponding electric field distributions of different volumes of adsorbent. The results show that 13.8 and 25.1 % of the input power could be dissipated if the adsorbent volume was increased to 0.71 and 1.47 mL, respectively. Even though the resonance frequencies of larger volumes of adsorbent were shifted to the lower frequencies, see **Figure 9 a**, they were still in the solid-state microwave generator's spectral band, which is from 2.43 to 2.47 GHz. Thus, the matching basically can be done by simply modifying the supplied frequency to the cavity. It was observed that less than 1 MHz deviation from the nominal frequency is sufficient to change the dissipated power by 14-27%. Cherbanski *et al.* [40] also observed the same behavior for the microwave heating of water in a single-mode applicator; they concluded that a minor 5 MHz deviation from the nominal frequency caused about 20% variation of the absorbed microwave power.

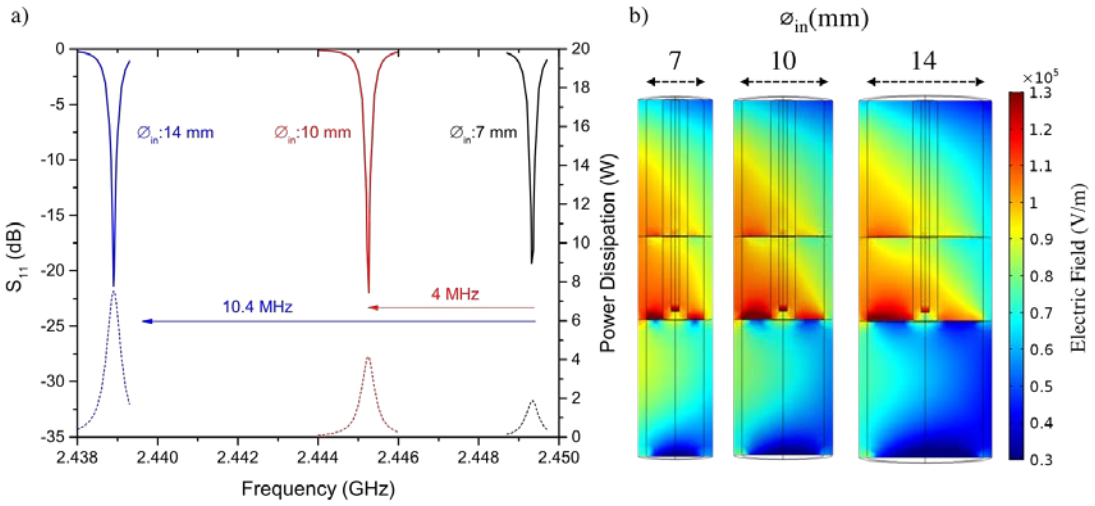

Figure 9. *Simulated a) reflection spectrum (S11 parameters) and power dissipation as a function of the excitation frequency with b) corresponding electric field distribution of larger volumes of absorbent with an input power of 30 W.*

As it was mentioned in the introduction the evolution of the dielectric properties with temperature would result in a temperature runaway in the sample that it could be predicted with the simulation. In **Figure 10** it could be observed that wehen the input power of the microwave cavity increases up to 38 W the temperature rises sharply after 210 s heated. This was also observed experimentally (not shown).

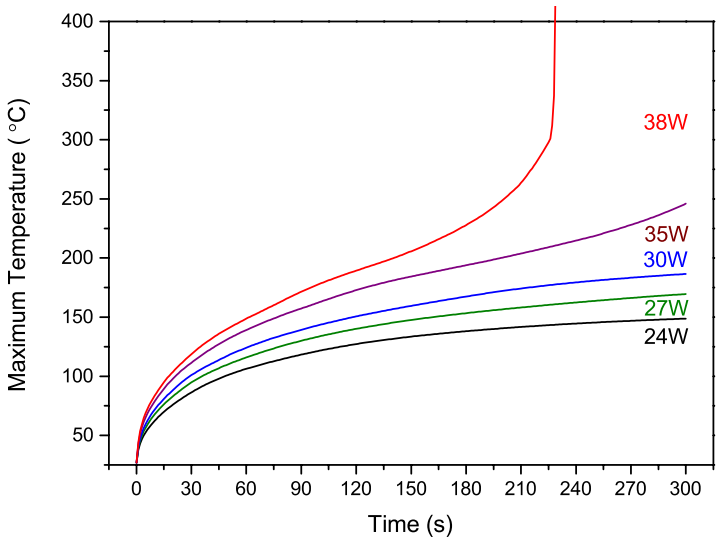

Figure 10. *Simulation of temperature evolution with time for different MW power.*

Different materials such as SiC, (ε'=16.9 and ε''=0.77, V:0.31mL) and CNTs (ε'=17.8 and ε''=26.4, V=0.31mL) were also employed in the simulation due to their relatively higher dielectric properties to NaY zeolite (ε'=1.3 and ε''=0.01, V:0.31mL). **Figure 11** represents the parametric sweep of two different samples. It was observed that 16.3 and 49.2% of the input power were dissipated in the CNTs and SiC fixed-beds, respectively. The electric field intensity decreased by two orders of magnitude, especially in the case of CNTs, see **Figure 11 b**. This is due to the high dielectric properties, which reduce the penetration depth of the electromagnetic waves into the load.

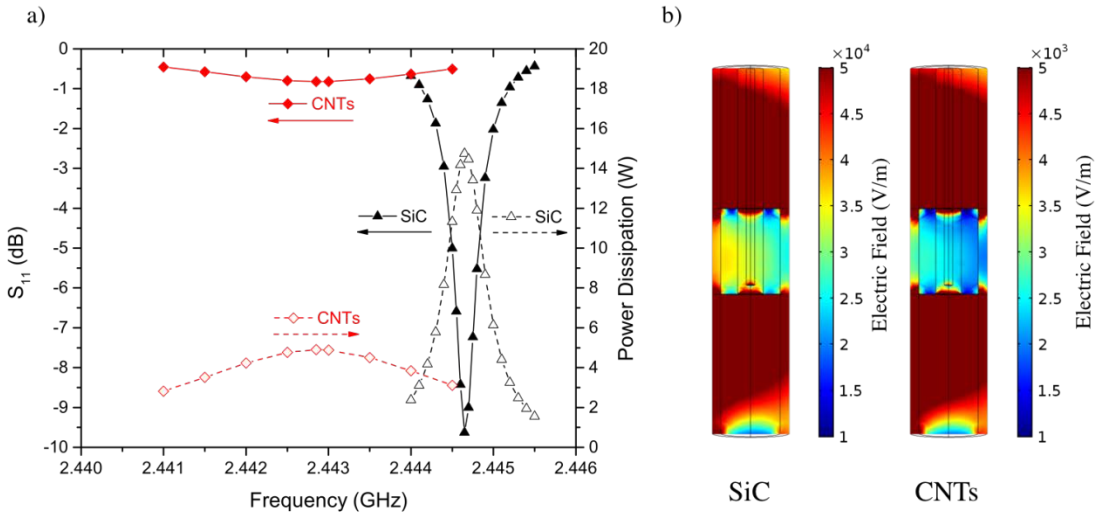

Figure 11. *Simulated a) reflection spectrum (S11 parameters) and power dissipation and b) corresponding electric field distribution of SiC and CNTs with an input power of 30 W (⌀in:7mm).*

5. Conclusions

In this study, microwave heating of dry porous NaY zeolite was investigated numerically and experimentally. A three-dimensional mathematical model of the microwave heating system with the fixed-bed tubular configuration was developed. Energy and momentum equations were solved together with Maxwell's equations using COMSOL Multiphysics® software. The electric field distribution in the microwave heating cavity, as well as in the fixed-bed, and the reflection spectrum were obtained. Furthermore, the transient temperature profiles of the zeolite and quartz tube were simulated on the basis of experimentally measured dielectric properties (ε' and ε'') as a function of temperature.

The numerical results of the reflection spectra and transient temperature profiles of the fixed-bed and quartz wall surface matched with the experimental data satisfactorily. An average percentage relative error of ±10.3% for the fixed-bed and ±13.4% for the quartz wall was observed. Due to the non-uniform electric field distribution within the sample, a temperature gradient was observed. Despite this gradient, 58% of the fixed bed has a temperature between 160-197ºC.

The overall energy balance shows that only 6.2% of the input power was dissipated within the sample. This lower efficiency was linked to the small volume of sample (0.31 mL) with regards to the whole cavity volume (2.8 L). The simulation results show that the efficiency of microwave heating cavity could be increased even further by using larger volumes of the NaY zeolite load, as well as heating materials with higher dielectric loss compared to zeolite such as SiC and CNTs.

Acknowledgements

Financial support from the European Research Council ERC-Advanced Grant HECTOR is gratefully acknowledged. Hakan Nigar acknowledges financial support from the Spanish Ministry of Education for the FPU grant (Formación del Profesorado Universitario – FPU12/06864), and also for the academic short stay grant (Estancia Breve – FPU2016) at the Delft University of Technology, Delft, The Netherlands.

REFENRECES

1. Bermúdez, J.M., et al., *Energy consumption estimation in the scaling-up of microwave heating processes.* Chemical Engineering and Processing: Process Intensification, 2015. **95**: p. 1-8.
2. Moseley, J.D. and C.O. Kappe, *A critical assessment of the greenness and energy efficiency of microwave-assisted organic synthesis.* Green Chemistry, 2011. **13**(4): p. 794-806.
3. Meredith, R.J. and E. Institution of Electrical, *Engineers' Handbook of Industrial Microwave Heating*. Energy Engineering Series. 1998: Institution of Electrical Engineers.
4. Xu, L., et al., *Study on characteristics of microwave melting of copper powder*. Journal of Alloys and Compounds, 2017. **701**: p. 236-243.
5. Stefanidis, G.D., et al., *A helicopter view of microwave application to chemical processes: reactions, separations, and equipment concepts.* Reviews in Chemical Engineering, 2014. **30**(3): p. 233-259.
6. Durka, T., et al., *Microwave-activated methanol steam reforming for hydrogen production.* International Journal of Hydrogen Energy, 2011. **36**(20): p. 12843-12852.
7. Sturm, G.S.J., et al., *On the effect of resonant microwave fields on temperature distribution in time and space.* International Journal of Heat and Mass Transfer, 2012. **55**(13–14): p. 3800-3811.
8. Sturm, G.S.J., et al., *On the parametric sensitivity of heat generation by resonant microwave fields in process fluids.* International Journal of Heat and Mass Transfer, 2013. **57**(1): p. 375-388.
9. Ramírez, A., et al., *Ethylene epoxidation in microwave heated structured reactors.* Catalysis Today, 2016. **273**: p. 99-105.
10. Horikoshi, S., et al., *Selective heating of Pd/AC catalyst in heterogeneous systems for the microwave-assisted continuous hydrogen evolution from organic hydrides: Temperature distribution in the fixed-bed reactor.* International Journal of Hydrogen Energy, 2016. **41**(28): p. 12029-12037.
11. Mimoso, R.M.C., et al., *Simulation and control of continuous glass melting by microwave heating in a single-mode cavity with energy efficiency optimization.* International Journal of Thermal Sciences, 2017. **111**: p. 175-187.
12. Lin, B., et al., *Sensitivity analysis on the microwave heating of coal: A coupled electromagnetic and heat transfer model.* Applied Thermal Engineering, 2017. **126**: p. 949-962.
13. Hong, Y.-d., et al., *Three-dimensional simulation of microwave heating coal sample with varying parameters.* Applied Thermal Engineering, 2016. **93**: p. 1145-1154.
14. Farag, S., et al., *Temperature profile prediction within selected materials heated by microwaves at 2.45GHz.* Applied Thermal Engineering, 2012. **36**: p. 360-369.
15. *COMSOL Multiphysics® v. 5.2. www.comsol.com. COMSOL AB, Stockholm, Sweden.*
16. MATLAB R2014b, The MathWorks, Inc. Natick, MA.
17. Catala-Civera, J.M., et al., *Dynamic Measurement of Dielectric Properties of Materials at High Temperature During Microwave Heating in a Dual Mode Cylindrical Cavity*. Microwave Theory and Techniques, IEEE Transactions on, 2015. **63**(9): p. 2905-2914.

18. Chen, W.-H., T.-C. Cheng, and C.-I. Hung, *Numerical predictions on thermal characteristic and performance of methanol steam reforming with microwave-assisted heating.* International Journal of Hydrogen Energy, 2011. **36**(14): p. 8279-8291.
19. Sturm, G.S.J., et al., *Microwaves and microreactors: Design challenges and remedies.* Chemical Engineering Journal, 2014. **243**: p. 147-158.
20. Pozar, D.M., *Microwave Engineering*. 2012, Wiley: Hoboken :.
21. *RF Module User's Guide, pp. 80-82. COMSOL Multiphysics® v. 5.2. www.comsol.com. COMSOL AB, Stockholm, Sweden.*
22. Sturm, G.S.J., et al., *Exploration of rectangular waveguides as a basis for microwave enhanced continuous flow chemistries.* Chemical Engineering Science, 2013. **89**: p. 196-205.
23. *Heat Transfer Module User's Guide, pp. 105-110. COMSOL Multiphysics® v. 5.2. www.comsol.com. COMSOL AB, Stockholm, Sweden.*
24. Legras, B., et al., *About using microwave irradiation in competitive adsorption processes.* Applied Thermal Engineering, 2013. **57**(1-2): p. 164-171.
25. *CFD Module User's Guide, pp. COMSOL Multiphysics® v. 5.2. www.comsol.com. COMSOL AB, Stockholm, Sweden.*
26. Nield, D.A. and A. Bejan, *Convection in Porous Media*. 2012: Springer New York.
27. Çengel, Y.A. and J.M. Cimbala, *Fluid Mechanics: Fundamentals and Applications, SI Version*. McGraw-Hill series in mechanical engineering. 2006: McGraw-Hill Education.
28. Legras, B., et al., *Mechanisms Responsible for Dielectric Properties of Various Faujasites and Linde Type A Zeolites in the Microwave Frequency Range.* The Journal of Physical Chemistry C, 2011. **115**(7): p. 3090-3098.
29. Gracia, J., et al., *Heating of Zeolites under Microwave Irradiation: A Density Functional Theory Approach to the Ion Movements Responsible of the Dielectric Loss in Na, K, and Ca A-Zeolites.* The Journal of Physical Chemistry C, 2013. **117**(30): p. 15659-15666.
30. Simon, U. and U. Flesch, *Cation-cation interaction in dehydrated zeolites X and Y monitored by modulus spectroscopy.* Journal of Porous Materials, 1999. **6**(1): p. 33-40.
31. Ohgushi, T. and M. Nagae, *Durability of Zeolite Against Repeated Activation Treatments with Microwave Heating.* Journal of Porous Materials, 2005. **12**(4): p. 265-271.
32. Tatsuo, O. and W. Akiko, *Simple suppressing method of thermal runaway in microwave heating of zeolite and its application.* PhysChemComm, 2001. **4**(3): p. 18-20.
33. Leong, K.C. and Y. Liu, *Numerical modeling of combined heat and mass transfer in the adsorbent bed of a zeolite/water cooling system.* Applied Thermal Engineering, 2004. **24**(16): p. 2359-2374.
34. Griesinger, A., K. Spindler, and E. Hahne, *Measurements and theoretical modelling of the effective thermal conductivity of zeolites.* International Journal of Heat and Mass Transfer, 1999. **42**(23): p. 4363-4374.
35. Jakubinek, M.B., B.-Z. Zhan, and M.A. White, *Temperature-dependent thermal conductivity of powdered zeolite NaX.* Microporous and Mesoporous Materials, 2007. **103**(1): p. 108-112.
36. Liu, Z.Y., et al., *Fast simple and accurate measurement of zeolite thermal conductivity.* Zeolites, 1990. **10**(6): p. 565-570.

37. Chen, W.-H., H.-J. Liou, and C.-I. Hung, *A numerical approach of interaction of methane thermocatalytic decomposition and microwave irradiation.* International Journal of Hydrogen Energy, 2013. **38**(30): p. 13260-13271.
38. Coss, P.M. and C.Y. Cha, *Microwave regeneration of activated carbon used for removal of solvents from vented air.* Journal of the Air and Waste Management Association, 2000. **50**(4): p. 529-535.
39. Cherbański, R., *Calculation of critical efficiency factors of microwave energy conversion into heat.* Chemical Engineering and Technology, 2011. **34**(12): p. 2083-2090.
40. Cherbański, R. and L. Rudniak, *Modelling of microwave heating of water in a monomode applicator – Influence of operating conditions.* International Journal of Thermal Sciences, 2013. **74**: p. 214-229.

Supporting Information

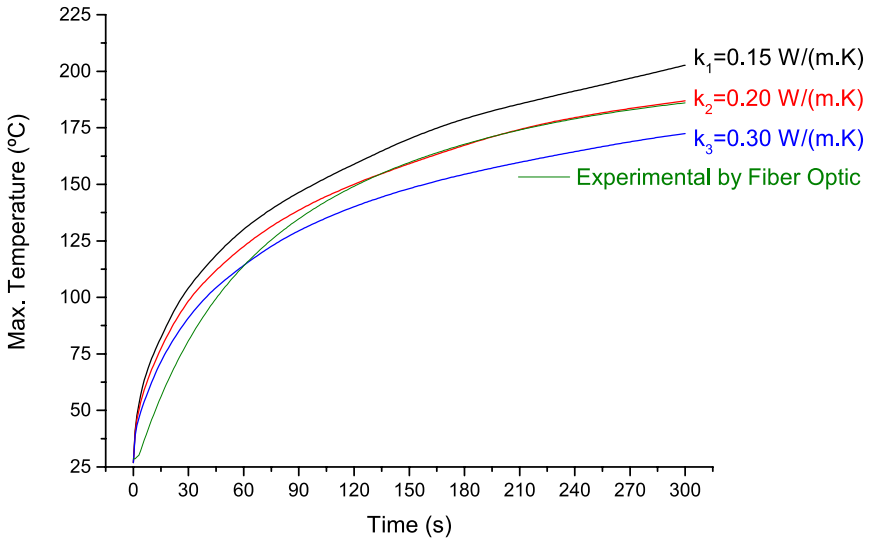

Figure S1. Simulated transient maximum temperature profiles of the fixed-bed with different thermal conductivities and measured data with the fiber optic